Theoretical Investigation on the Molecular Structure, Electronic, Spectroscopic Studies and Nonlinear Optical Properties of 5-bromo-1-(2-cyano-pyridin-4-yl)-1H-indazole-3-carboxylic acid diethylamide: a DFT and TD-DFT Study

A. Eşme
Department of Elementary Science Education, Faculty of Education, Kocaeli University, 41380, Umuttepe, Kocaeli, Turkey

(Received June 5, 2018; revised version April 5, 2019; in final form July 26, 2019)

The optimized structural parameters (bond lengths and bond angles), electronic, NLO, and spectroscopic properties (FT-IR, UV ^{1}H and ^{13}C NMR) of 5-bromo-1-(2-cyano-pyridin-4-yl)-1H-indazole-3-carboxylic acid diethylamide were investigated by the B3LYP, B3PW91, and BPV86 level of theory with the 6-311++G(d,p) basis set and were compared with the experimental values. The characterization of the covalent bond was carried out with the Wiberg bond indices (WBIs) derived through the natural bond orbital analysis. The complete vibrational frequencies have been made on the basis of the potential energy distribution (PED) obtained by the Vibrational Energy Distribution Analysis 4 (VEDA4) program. Moreover, the electronic properties, such as the energies of the frontier molecular orbitals (HOMO and LUMO), energy gap ($\Delta E_{\mathrm{LUMO-HOMO}}$), global reactivity descriptors (global hardness, global softness, chemical potential, and electrophilicity index), absorption wavelengths (λ), excitation energies (E) and oscillator strengths (f) were performed by the time-dependent density functional theory (TD-DFT) in the chloroform solvent and gas phase. The major contributions to the electronic transitions for the UV-Vis analysis were obtained using the Gauss-Sum 2.2 program Solvent effects on NMR tensors of the title compound have been investigated at the B3LYP, B3PW91, and BPV86 levels using the chloroform solvent and gas phase The weak interaction (Van der Waals), strong attraction (hydrogen bond) and strong repulsion (steric effect) in the title compound were analyzed via the reduced density gradient (RDG) analysis using Multiwfn software.

DOI: 10.12693/APhysPolA.136.378

PACS/topics: 5-bromo-1-(2-cyano-pyridin-4-yl)-1H-indazole-3-carboxylic acid diethylamide, NLO, NMR, vibrational spectra, UV, RDG

1. Introduction

Indazoles are an important class of bicyclic nitrogen-containing aromatic heterocycles and have attracted a great deal of attention in the past as well as in recent years due to their wide variety of biological properties. The indazoles represent an important subunit in drugs with a broad range of biological activities including antibacterial [1], antifungal [2], antiviral [3], antihypertensive [4], anticancer [5], anti-inflammatory [6], and immunomodulatory [7]. Indazoles with pyridine substituted compounds also have anti-cancer properties [8].

Recently, the 5-bromo-1-(2-cyano-pyridin-4-yl)-1H-indazole-3-carboxylic acid diethylamide was synthesized and characterized with its FT–IR, ^{1}H NMR, ^{13}C NMR spectroscopy and X-ray diffraction studies [9]. However, to the best of our knowledge, no literature is yet available on the structural properties and FT–IR, ^{1}H NMR, ^{13}C NMR, and UV-Vis spectroscopic techniques to fully determine the molecular structure by the DFT methods. In this case, molecular geometry, vibrational spectra (FT–IR), nuclear magnetic resonance (^{1}H and ^{13}C NMR) and NLO analysis, Mulliken and natural bond orbital (NBO) on atomic charges, molecular electrostatic potential map (MEP) surface of the investigated molecule have examined at the B3LYP, B3PW91, and BPV86 levels of the density functional theory with the 6-311++G(d,p) basis set. The total energy, HOMO and LUMO energies, the $\Delta E_{\mathrm{LUMO-HOMO}}$ energy gap, global reactivity descriptors like global hardness (η), global softness (σ), chemical potential (P_i), and electrophilicity index (ω) calculations in chloroform solvent and gas phase, and ultraviolet and visible light (UV-Vis) analysis were calculated with the TD-DFT calculations. The essence of this study is briefly to investigate solvent effects on NMR of the title compound using the B3LYP, B3PW91, and BPV86 levels with the 6-311++G(d,p) basis set in the chloroform solvent and gas phase. Reduced density gradient (RDG) of the title compound using the B3LYP/6-311++G(d,p) level was graphed which showed related interaction in the molecule.

corresponding author; e-mail: asli.esme@kocaeli.edu.tr

The non-covalent interactions of the title compound were studied using the reduced density gradient (RDG) analysis of which filled color map of electron density diagram was plotted using the B3LYP/6-311++G(d,p) level.

2. Computational details

All calculations were performed using the Gaussian 09 Rev. A 11.4 package program [10], and the obtained results were visualized by the Gauss View Rev. 5.0.9 software [11]. The molecular structure of the title molecule in the ground state was optimized using the Density Functional Theory (DFT) with the Becke–3–Lee–Yang–Parr (B3LYP) functional [12, 13], B3PW91 [14–16], and BPV86, which uses Perdew's 1986 functional with local correlation replaced by what was suggested Vosko et al. [17–19] combined with the 6-311++G(d,p) basis set (referred to as "large" basis). Moreover, the molecular structure of the title molecule was studied using the B3LYP, B3PW91, and BPV86 levels with the 6-311++G(d,p) basis set. The Wiberg bond indece (WBI) [20] which is closely related to the bond character was obtained from the natural bond orbital (NBO) analysis [21] as implemented in Gaussian 09 with keyword "pop = nboread". Detailed assignments of vibrational modes were carried out based on percentage potential energy distribution (PED) analysis using the VEDA4 program written by Jamroz [22]. The scale factors were used to obtain the best agreement results between the calculated and experimental frequencies. The vibrational frequencies for the title compound were calculated with the B3LYP, B3PW91, and BPV86 levels with 6-311++G(d,p) basis set and then computed frequencies were scaled by 0.9617, 0.966, and 1.014, respectively [23 – 25]. The functions such as RDG and $\mathrm{sgn}(\lambda_2)\rho$ were calculated with Multiwfn [26], and plotted with VMD program [27], respectively.

In order to evaluate the agreement of different levels of theory (B3LYP, B3PW91, and BPV86) and experimental data for the title compound , the linear correlation coefficients (R^2), the overall mean percent deviation (MPD), and the root mean square deviation (RMSD) values for structural and vibrational properties were defined as follows [28]. The overall mean percent deviation,

$$\mathrm{MPD} = \frac{\sum_{i=1}^{n} \left(\left| \delta_i^{\mathrm{theo}} - \delta_i^{\mathrm{exp}} \right| / \delta_i^{\mathrm{exp}} \right)}{n} \times 100. \qquad (1)$$

The root mean square deviation,

$$\mathrm{RMSD} = \sqrt{\frac{\sum_{i=1}^{n} \left(\upsilon_i^{\mathrm{theo}} - \upsilon_i^{\mathrm{exp}} \right)^2}{n}}, \qquad (2)$$

where δ_i^{theo}, $\upsilon_i^{\mathrm{theo}}$ and δ_i^{exp}, $\upsilon_i^{\mathrm{exp}}$ are i-th theoretical and corresponding experimental values, respectively, and n is the number of the experimental or calculated data.

3. Results and discussion

3.1. Structural analysis

The 5-bromo-1-(2-cyano-pyridin-4-yl)-1H-indazole-3-carboxylic acid diethylamide ($C_{18}H_{16}BrN_5O$) belongs to triclinic system, with the $P\bar{1}$ space group and the unit cell parameters a=11.2330(2) Å, b=11.6130(2) Å, c=15.4710(3) Å, and V=1788.45(6) Å^3 [9]. The title molecule possesses 5-bromo-1H-indazole core with 2-cyano-pyridine and carboxylic acid diethylamide substituents on the pyrazole ring. The single crystal structure and optimized geometries by the B3LYP, B3PW91, and BPV86 levels of theory with the 6-311++G(d,p) basis set of the title molecule with atom numbering are shown in Fig. 1. The selected theoretical optimized structural parameters such as bond lengths and bond angles of the title compound are obtained with the DFT (B3LYP, B3PW91, and BPV86) methods with the 6-311++G(d,p) basis set as compared to experimental results observed from X-ray crystallography [9] and the results are tabulated in Table I.

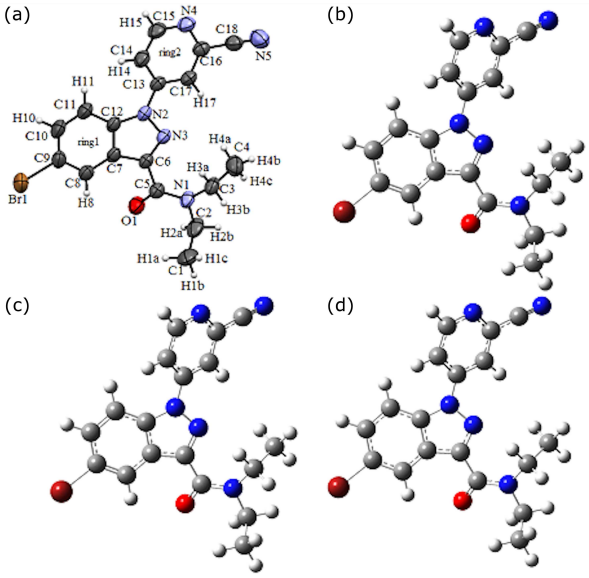

Fig. 1. The single crystal structure [9] (a) the optimized molecular structure obtained at the B3LYP (b) B3PW91 (c) and BPV86 (d) levels with the 6-311++G(d,p) basis set of the title compound .

A notable difference among the methods occurs in the computed C–N, C=N and C≡N bond lengths. From Table I, it is found that the C12–N2, C6=N3 bond lengths in the pyrazole ring and C15–N4, C16=N4 bond lengths in 2-cyano-pyridine ring were found to be 1.383(3), 1.304(3) Å and 1.325(4), 1.331(4) Å from the X-ray [9], respectively. The computed bond lengths were calculated at 1.389, 1.384, 1.396 Å and 1.317, 1.315, 1.331 Å for the C12–N2 and C6=N3 distances in the pyrazole ring and at 1.331, 1.328, 1.340 Å and

TABLE I

Optimized geometrical parameters and Wiberg bond indeces (WBIs) in parenthesis (from NBO) of the title compound calculated at the B3LYP, B3PW91, and BPV86 levels with the 6-311++G(d,p) basis set.

Parameters	Exp. [9]	B3LYP	B3PW91	BPV86
Bond lengths [Å]				
C1–C2	1.490(6)	1.530(1.024)	1.523(1.007)	1.533(1.007)
C2–N1	1.462(4)	1.473(0.933)	1.465(0.933)	1.476(0.935)
C3–N1	1.457(4)	1.470(0.940)	1.462(0.939)	1.473(0.942)
C3–C4	1.491(5)	1.530(1.022)	1.524(1.004)	1.533(1.008)
C5–O1	1.225(3)	1.232(1.590)	1.229(1.581)	1.244(1.578)
C5–N1	1.338(3)	1.362(1.215)	1.358(1.238)	1.371(1.240)
C5–C6	1.490(4)	1.500(0.991)	1.495(0.983)	1.500(0.988)
C6–N3	1.304(3)	1.317(1.568)	1.315(1.574)	1.331(1.561)
C6–C7	1.425(3)	1.440(1.167)	1.436(1.159)	1.444(1.164)
C7–C8	1.385(4)	1.404(1.299)	1.401(1.284)	1.409(1.288)
C7–C12	1.389(4)	1.410(1.274)	1.407(1.297)	1.419(1.274)
C8–C9	1.359(4)	1.381(1.477)	1.379(1.477)	1.390(1.467)
C9–C10	1.391(5)	1.408(1.335)	1.407(1.307)	1.414(1.322)
C9–Br1	1.895(3)	1.917(1.039)	1.901(1.043)	1.918(1.049)
C10–C11	1.362(5)	1.385(1.489)	1.382(1.558)	1.393(1.582)
C11–C12	1.400(4)	1.401(1.319)	1.399(0.976)	1.406(1.499)
C12–N2	1.383(3)	1.389(1.087)	1.384(1.090)	1.396(1.092)
C13–C17	1.376(4)	1.398(1.353)	1.395(1.346)	1.404(1.343)
C13–C14	1.381(4)	1.396(1.374)	1.394(1.360)	1.404(1.351)
C13–N2	1.403(4)	1.406(1.025)	1.401(1.035)	1.409(1.041)
C14–C15	1.368(4)	1.394(1.419)	1.392(1.422)	1.400(1.423)
C15–N4	1.325(4)	1.331(1.441)	1.328(1.422)	1.340(1.422)
C16–N4	1.331(4)	1.342(1.361)	1.339(1.368)	1.353(1.364)
C16–C17	1.367(4)	1.394(1.404)	1.392(1.399)	1.402(1.394)
C16–C18	1.446(4)	1.442(1.063)	1.439(1.051)	1.442(1.060)
C18–N5	1.128(4)	1.154(2.874)	1.154(2.880)	1.167(2.871)
N2–N3	1.371(2)	1.365(1.141)	1.356(1.130)	1.374(1.133)
R_2		0.99666	0.99650	0.99593
MPD		1.22099	0.97750	1.69551
RMSD		0.01975	0.01652	0.08140
Bond angles [°]				
N1–C2–C1	112.7(3)	113.05	113.00	112.92
O1–C5–C6	116.6(2)	116.66	116.79	116.98
N1–C3–C4	113.2(3)	113.52	113.51	113.37
O1–C5–N1	122.3(3)	122.07	122.21	121.93
N1–C5–C6	121.2(3)	121.27	121.00	121.09
C3–N1–C2	117.2(2)	116.29	116.38	116.35
C5–N1–C3	126.4(2)	126.84	126.75	126.90
C5–N1–C2	116.1(2)	116.69	116.65	116.63
N3–C6–C7	111.4(2)	110.66	110.66	110.76
N3–N2–C12	110.5(2)	111.08	111.33	111.39
N3–C6–C5	125.1(2)	125.45	125.46	125.58
C7–C6–C5	123.2(3)	123.78	123.75	123.57
C8–C7–C6	133.3(3)	134.35	134.39	134.25
C12–C7–C6	104.9(2)	104.91	104.80	105.04
C8–C7–C12	121.8(2)	120.73	120.79	120.68
C9–C8–C7	117.4(3)	117.17	117.11	117.08
C6–N3–N2	106.8(2)	107.42	107.35	106.99
N3–N2–C13	116.9(2)	118.82	118.87	118.73
C8–C9–Br1	118.9(2)	119.46	119.50	119.39
C11–C10–C9	121.6(3)	120.93	121.01	120.84
C8–C9–C10	121.5(3)	122.28	122.24	122.43
N2–C12–C7	106.4(2)	105.91	105.84	105.80
C10–C9–Br1	119.6(2)	118.25	118.25	118.17
C7–C12–C11	119.9(3)	121.43	121.48	121.53
C10–C11–C12	117.7(3)	117.43	117.34	117.40
C17–C13–N2	119.5(2)	119.72	119.68	119.66
N2–C12–C11	133.7(3)	132.57	132.58	132.56
C15–C14–C13	119.1(3)	118.45	118.36	118.36
C17–C13–C14	117.1(3)	118.34	118.44	118.42
N4–C16–C17	125.8(3)	124.43	124.59	124.64
C14–C13–N2	123.3(3)	121.92	121.87	121.90
C17–C16–C18	119.3(3)	118.90	118.77	118.81
N4–C15–C14	125.3(3)	124.29	124.38	124.63
N5–C18–C16	178.8(4)	178.23	178.23	178.28
N4–C16–C18	114.8(3)	116.66	116.64	116.54
C16–C17–C13	118.6(3)	118.01	117.87	117.95
C12–N2–C13	132.2(2)	130.09	129.79	129.88
C15–N4–C16	114.1(3)	116.46	116.35	115.98
R_2		0.99641	0.99628	0.99656
MPD		0.66844	0.68407	0.66208
RMSD		0.99497	1.01203	0.94575

TABLE I cont.

1.342, 1.339, 1.353 Å for the C15–N4 and C16=N4 distances in the 2-cyano-pyridine ring using the B3LYP, B3PW91, and BPV86 methods with the 6-311++G(d,p) basis set of the title compound, respectively. The obtained C12–N2, C6=N3 bond lengths in the pyrazole ring are shorter than the C–N (1.443 Å) single bond length and are significantly longer than the C=N (1.269 Å) double bond length which suggests a degree of electron delocalization, but it is consistent with related structures [29, 30]. The obtained C–N bond lengths for the title compound correspond well to the delocalization of the C–N single and double bonds (1.390(2) and 1.367(3) Å), respectively, in the pyrazole ring of the compound 4,6-bis(4-flurophenyl)-2-phenyl-1H-indazol-3(2H)-one reported in the literature [31]. The calculated C16=N4 bond length is longer than C15–N4. This is because the substituent group is attached to the C16=N4 double bond. In our calculations, at the B3LYP, B3PW91, and BPV86 methods with the 6-311++G(d,p) basis set, the cyano group C18≡N5 bond length in 2-cyano-pyridine for the title compound is 1.154, 1.154, and 1.167 Å, respectively, whereas this C18≡N5 triple bond distance of the title compound is 1.128(4) Å [9]. These results confirm linearity which is quite a common feature observed in carbonitrile compounds [32].

The experimental N2–N3 (1.371(2) Å) bond length in the pyrazole ring of the title compound is indicative of partial N–N single bond character [33] and this bond length was calculated to be 1.365 Å for the B3LYP, 1.356 Å for the B3PW91, and 1.374 Å for the BPV86. The bond length of N–N in the pyrazole ring is calculated as 1.36 Å using the B3LYP/6-311++G(d,p) method [33].

As can be seen from Table I, the experimental C5=O1 bond length of the carboxylic acid diethylamide is found to be 1.225(3) Å [9], whereas the calculated bond length with the B3LYP, B3PW91, and BPV86 levels with the 6-311++G(d,p) basis set of the title compound is 1.232, 1.224, and 1.244 Å respectively. Therefore it has partial double-bond character [34]. The C=O bond length of amide-1 compound was calculated at 1.229 Å for the B3LYP/6-31G++(d,p) method by Alver et al. [35].

The Wiberg bond index (WBI) revealing the strength of the covalent character, was provided by natural bond orbital (NBO) analysis. The calculated Wiberg bond indices [20] for the title compound are given within parenthesis and compared in Table I. The WBIs of the N2–N3 /C12–N2 bonds in the pyrazole ring were calculated to be 1.141/1.087 (B3LYP), 1.130/1.090 (B3PW91), 1.133 / 1.092 (BPV86), which are very close to a covalent single bond (1.0). NBO analysis resulted in WBIs values smaller than the typical covalent double bond (2.0) for C16=N4, C6=N3 bonds ($\sim$ 1.364, $\sim$ 1.568). The calculated WBI of C18≡N5 bond in 2-cyano-pyridine ring for the title compound using B3LYP, B3PW91, and BVP86 methods was found to be $\sim$ 2.875, which is very close to a covalent triple bond (3.0). Since a smaller WBI generally intimates a weaker bond, C2–N1 and C3–N1 are found to be similar ($\sim$ 0.933 and $\sim$ 0.940), respectively. Thus these bonds are interpreted as a weak covalent single bond.

The selected bond angles are summarized in Table I. The bond angle O1–C5–N1 is 122.3(3)°. The bond angle O1–C5–N1 calculated by the B3LYP, B3PW91, and BVP86 methods with the 6-311++G(d,p) basis set of the title compound is 122.07°, 122.21°, and 121.93°, respectively. The bond angle determined from BPV86 method is slightly lower than that obtained from B3LYP and B3PW91 methods.

In order to compare the theoretical results with the experimental results, the linear correlation coefficients (R^2), the overall mean percent deviation (MPD), and the root mean square deviation (RMSD) values obtained with the B3LYP, B3PW91, and BPV86 methods at the 6-311++G(d,p) basis set for the title compound. A comparison of the calculated and experimental optimized geometric parameters is given in Table I. As the criteria of agreement the R^2, MPD, and RMS values were applied. The R^2, MPD and RMSD values have been obtained in the ranges 0.99666–0.99593, 0.97750–1.69551 and 0.01652–0.08140 (for bond lengths), and 0.99628-0.99656, 0.66208–0.68407 and 0.94575–1.01203 (for bond angles) of the title compound, respectively. To assess the performance of all used hybrid DFT methods in the prediction of the bond lengths and angles of the title compound, the ranking of these methods for the linear correlation coefficients, the overall mean percent deviation, and the root mean square deviation is: B3LYP > B3PW91 > BPV86 (for bond lengths) and BPV86 > B3LYP > B3PW91 (for bond angles), BPV86 > B3LYP > B3PW91 (for bond lengths), B3PW91 > B3LYP > BPV86 (for bond angles), BPV86 > B3LYP > B3PW91 (for bond lengths), and B3PW91 > B3LYP > BPV86 (for bond angles), respectively.

The comparative graphs of bond lengths and bond angles of the title molecule are presented in Fig. 2.

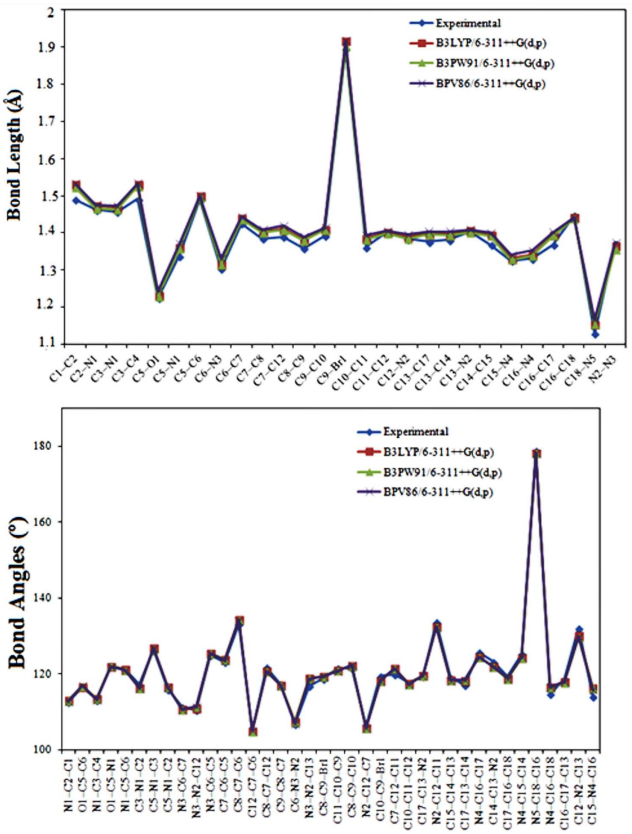

Fig. 2. The bond length and bond angle difference between theoretical (B3LYP, B3PW91, and BPV86) approaches.

3.2. Vibrational analysis

The theoretically predicted unscaled and scaled vibrational frequencies of the title compound are computed using the B3LYP, B3PW91, and BPV86 functionals with the 6-311++G(d,p) basis set. Their assignments along with potential energy distribution (PED) contributions performed by means of VEDA 4 program [22] are presented in Table II in comparison with the experimental [9] results. The calculated assignments are slightly different from the experimental values of the normal modes. Thus, the obtained frequencies were scaled by 0.9668 at the B3LYP/6-311++G(d,p) level [36], 1.014 at the BPV86/6-311++G(d,p) level [37], and 0.966 at the B3PW91/6-311++G(d,p) [38], respectively. The experimental and computational IR spectra plotted for comparison purpose are shown in Fig. 3.

TABLE II

Comparison of the observed FT-IR spectra [9] and calculated vibrational wavenumbers with potential energy distribution (PED) using the B3LYP, B3PW91, and BPV86 methods with 6-311++G(d,p) basis set of the title compound.

No.	Assignments	Exp. [9]	B3LYP			B3PW91			BPV86		
		FT-IR	PED [%]	Unscaled	Scaled	PED [%]	Unscaled	Scaled	PED [%]	Unscaled	Scaled
1	$\nu_s(CH)_{Ring1}$	3436.79	99	3235.39	3127.98	99	3241.57	3131.36	99	3159.62	3203.85
2	$\nu_s(CH)_{Ring2}$	99	3232.03	3124.73	99	3239.64	3129.49	99	3155.28	3199.46	
3	$\nu_s(CH)_{Ring1,2}$	95	3226.17	3119.06	95	3231.80	3121.92	92	3148.19	3192.27	
4	$\nu_s(CH)_{Ring1,2}$	99	3215.56	3108.80	99	3223.79	3114.18	98	3140.76	3184.73	
5	$\nu_{as}(CH)_{Ring1}$	98	3199.83	3093.60	99	3208.30	3099.22	98	3127.34	3171.12	
6	$\nu_{as}(CH)_{Ring2}$	3102.34	98	3164.66	3059.59	98	3172.87	3064.99	98	3087.46	3130.68
7	$\nu_{as}(CH_2)$	88	3139.84	3035.60	73	3146.38	3039.40	68	3063.17	3106.05	
8	$\nu_{as}(CH_2)$, $\nu_{as}(CH_3)$	32, 57	3124.11	3020.39	33, 62	3138.84	3032.12	17, 69	3057.98	3100.79	
9	$\nu_{as}(CH_3)$	88	3117.52	3014.02	81	3134.03	3027.47	80	3052.74	3095.48	
10	$\nu_{as}(CH_3)$, $\nu_{as}(CH_2)$	62, 36	3110.48	3007.22	44, 48	3125.37	3019.11	42, 48	3043.37	3085.98	
11	$\nu_{as}(CH_3)$	2983.92	96	3091.21	2988.58	92	3110.67	3004.91	90	3030.55	3072.98
12	$\nu_{as}(CH_3)$	2961.28	89	3086.70	2984.22	82	3106.18	3000.57	72	3026.88	3069.26
13	$\nu_s(CH_2)$	93	3058.38	2956.84	96	3065.79	2961.55	96	2983.36	3025.13	
14	$\nu_s(CH_3)$	95	3029.86	2929.27	77	3043.94	2940.45	99	2967.67	3009.22	
15	$\nu_s(CH_3)$	2935.07	97	3033.56	2932.85	87	3040.22	2936.85	94	2966.32	3007.85
16	$\nu(C\equiv N)$	2239.94	90	2346.48	2268.58	89	2356.86	2276.73	89	2252.82	2284.36
17	$\nu(C=O)$	1623.50	77	1671.50	1616.01	78	1697.69	1639.97	76	1614.54	1637.14
18	$\nu(CC)_{Ring1}$	62	1636.53	1582.20	66	1654.76	1598.50	60	1586.75	1608.97	
19	$\nu(CC)_{Ring2}$	1586.24	56	1621.87	1568.02	59	1638.07	1582.38	57	1569.30	1591.27
20	$\nu(CC)_{Ring1,2}$	1557.06	31	1610.73	1557.25	33	1627.96	1572.61	45	1560.63	1582.45
21	$\nu(CC)_{Ring1,2}$	1509.33	32	1592.82	1539.94	33	1609.97	1555.23	34	1543.43	1565.04
22	$\nu(CC)$, $\nu(NC)_{Ring1}$	1479.92	11, 33	1530.92	1480.09	13, 33	1549.73	1497.04	11, 24	1473.13	1493.75
23	$\sigma(CH_2)$	42	1511.16	1460.99	11	1514.46	1462.97	11	1457.77	1478.18	
24	$\sigma(CH_3)$, $\gamma(HCCN)$	64, 11	1506.21	1456.20	57, 10	1499.09	1448.12	51, 10	1454.77	1475.14	
25	$\sigma(HCN)$	15	1502.03	1452.16	17	1508.39	1457.11	10	1449.79	1470.09	
26	$\delta(CH_3)$	46	1494.44	1444.83	46	1488.94	1438.32	22	1448.30	1468.58	
27	$\delta(CH_3)$	61	1491.64	1442.12	46	1484.31	1433.84	24	1445.50	1465.74	
28	$\sigma(CH_2)$	1424.40	10	1484.19	1434.92	14	1471.82	1421.78	17	1435.61	1455.71
29	$\sigma(CH_2)$	48	1480.30	1431.15	21	1468.73	1418.79	45	1423.57	1443.50	
30	$\sigma(HCC)$, $\nu(NC)_{Ring1}$	1379.70	10, 14	1445.65	1397.65	14, 13	1451.01	1401.68	12, 31	1393.59	1413.10
31	$\beta(CH_3)$	1364.06	64	1411.69	1364.82	37	1404.22	1356.48	64	1359.81	1378.85
32	$\beta(CH_3)$	36	1399.48	1353.02	11	1390.46	1343.18	35	1355.52	1374.50	
33	$\delta(HCC)$	1347.03	12	1398.34	1351.92	10	1381.33	1334.37	17	1337.56	1356.29
34	$\tau(HCNC)$	1322.78	55	1381.48	1335.62	50	1371.86	1325.22	56	1329.72	1348.34
35	$\beta(CH_2)$, $\beta(HCN)$	1295.21	23, 25	1338.42	1293.98	26, 24	1339.02	1293.49	26, 22	1294.54	1312.66
36	$\beta(HCN)$, $\nu(NC)_{Ring2}$	1276.04	41, 26	1316.86	1273.14	33, 12	1316.88	1272.11	35, 12	1271.23	1289.03
37	$\nu(NC)_{Ring2}$	10	1305.17	1261.84	12	1297.48	1253.37	11	1252.48	1270.02	
38	$\delta(HCC)$	1249.63	14	1274.04	1231.74	17	1274.92	1231.57	24	1206.60	1223.49
39	$\nu(NC)$	1215.73	32	1235.98	1194.95	34	1245.26	1202.92	35	1195.60	1212.34
40	$\delta(HCC)$, $\nu(NN)$	1181.40	18, 14	1199.65	1159.82	17, 22	1207.21	1166.17	25, 16	1140.81	1156.78
41	$\sigma(HCC)$	1156.82	44	1179.05	1139.91	49	1177.88	1137.83	43	1096.80	1112.16
42	$\delta(HCC)$, $\nu(NN)$	1126.23	31, 21	1134.91	1097.23	19, 25	1143.95	1105.06	11, 32	1080.82	1095.95
43	$\gamma(HCCN)$	1095.67	31	1115.55	1078.51	32	1114.24	1076.36	30	1078.57	1093.67
44	$\sigma(CCN)$, $\gamma(HCCN)$	1072.01	11, 23	1099.55	1063.05	11, 21	1100.12	1062.72	10, 20	1063.68	1078.57
45	$\nu(CC)$	15	1087.67	1051.56	18	1092.77	1055.62	12	1053.40	1068.15	
46	$\delta(HCC)$	1044.71	15	1063.60	1028.29	17	1068.06	1031.75	30	1029.94	1044.36
47	$\nu(CC)$, $\nu(NC)$	992.36	22, 11	1017.06	983.29	23, 12	1027.00	992.08	23, 11	990.47	1004.34
48	$\sigma(CCN)$, $\sigma(CNC)$	40, 14	1007.05	973.62	42, 14	1009.32	975.00	34, 11	972.66	986.28	
49	$\tau(HCNC)$, $\tau(HCCN)$	942.08	63, 19	992.07	959.13	63, 19	991.62	957.90	64, 18	946.51	959.76
50	$\sigma(CCC)$	23	982.94	950.31	25	987.98	954.39	10	955.81	969.19	

TABLE II cont.

No.	Assignments	Exp. [9]	B3LYP			B3PW91			BPV86		
		FT-IR	PED [%]	Unscaled	Scaled	PED [%]	Unscaled	Scaled	PED [%]	Unscaled	Scaled
51	τ(HCCC), τ(HCCN)	44, 32	965.46	933.41	44, 32	963.72	930.95	48, 37	917.55	930.40	
52	ν(CC)	56	948.34	916.86	52	955.62	923.13	52	924.41	937.35	
53	τ(HCCC)	74	923.19	892.54	75	916.91	885.74	75	877.97	890.26	
54	τ(HCCN)	881.70	72	913.48	883.15	71	912.34	881.32	71	869.88	882.06
55	ω(HCCN)	847.29	13	864.01	835.32	26	866.89	837.42	53	823.66	835.19
56	τ(HCCN)	824.07	15	856.98	828.53	29	859.17	829.96	15	780.89	791.82
57	ω(HCCC), ω(HCCN)	795.57	35, 46	810.97	784.05	35, 45	810.07	782.53	33, 45	772.63	783.45
58	γ(ONCC)	32	797.78	771.29	37	797.64	770.52	15	762.71	773.39	
59	γ(HCNC), τ(HCCN)	14, 21	788.07	761.91	0, 23	783.06	756.44	13, 17	758.88	769.50	
60	γ(HCCN), γ(HCNC)	741.33	20, 15	784.11	758.08	26, 10	779.42	752.92	11, 15	751.10	761.62
61	τ(CCNC), τ(CNCC)	17, 28	756.93	731.80	12, 20	759.30	733.48	30, 16	726.54	736.71	
62	γ(ONCC), τ(NCCC)	682.42	32, 20	738.86	714.33	29, 20	739.28	714.14	20, 20	704.19	714.05
63	β(CNC), β(CCC)	671.58	15, 12	680.35	657.76	16, 13	681.14	657.98	12, 11	658.53	667.75
64	τ(CCNC), τ(NCCC)	638.56	17, 24	660.93	638.99	17, 24	664.23	641.65	16, 20	635.59	644.49
65	β(CCC)	607.27	10	615.03	594.61	11	616.05	595.10	13	594.84	603.17
66	β(CCC)	574.80	21	596.73	576.92	21	594.87	574.64	14	576.68	584.75
67	τ(CCCC), τ(NCCC)	37, 15	580.51	561.24	39, 14	582.67	562.86	33, 12	559.80	567.64	
68	β(NCC)	30	577.88	558.69	31	578.30	558.64	18	557.14	564.94	
69	σ(CCN)	509.39	48	510.32	493.38	42	509.90	492.56	42	494.91	501.84
70	τ(NCCC), τ(CCNC)	488.77	32, 20	499.66	483.07	33, 19	499.77	482.78	13, 17	480.45	487.18
71	ν(CC), σ(CNC)	28, 11	489.02	472.78	27, 11	488.33	471.73	23, 11	473.56	480.19	
72	σ(OCC)	13	462.42	447.07	13	463.07	447.33	11	446.29	452.54	
73	τ(CCCC)	30	437.01	422.50	27	435.52	420.71	11	420.39	426.28	
74	σ(OCC), σ(CNC)	13, 29	432.23	417.88	11, 28	430.64	416.00	11, 13	417.15	422.99	
75	τ(NCCC), τ(CCNC)	46, 16	378.81	366.23	45, 16	377.69	364.85	43, 20	359.05	364.08	
76	ν(BrC)	22	342.94	331.55	22	345.45	333.70	21	333.36	338.03	
77	σ(CCN)	42	332.56	321.52	41	330.12	318.90	43	323.11	327.63	
78	γ(BrCCC)	14	299.77	289.82	15	300.77	290.54	13	289.82	293.88	
79	σ(CCN)	10	277.00	267.80	11	277.21	267.78	10	267.20	270.94	
80	σ(BrCC)	19	259.91	251.28	19	258.18	249.40	19	251.91	255.44	
81	γ(HCCN)	44	225.93	218.43	41	225.39	217.73	48	219.56	222.63	
82	γ(HCCN)	13	214.88	207.75	11	213.72	206.45	12	211.23	214.19	
83	σ(BrCC)	12	185.07	178.93	12	183.61	177.37	12	180.14	182.66	
84	σ(C≡N)	13	152.54	147.48	12	152.72	147.53	13	147.02	149.09	
85	τ(CCCC), γ(CCNC)	32, 28	144.82	140.01	31, 28	144.66	139.74	0, 31	140.29	142.25	
86	σ(C≡N)	14	137.96	133.38	14	137.61	132.93	14	132.21	134.06	
87	γ(CCCN)	24	129.26	124.97	24	128.69	124.31	22	124.73	126.48	
88	γ(BrCCC)	15	101.19	97.83	16	100.50	97.08	17	96.86	98.22	
89	σ(CCN)	19	92.72	89.64	15	95.03	91.80	18	87.37	88.59	
90	γ(CCNC)	26	77.88	75.29	28	77.35	74.72	32	74.15	75.19	
91	γ(NCCC)	62	12.80	12.38	64	10.62	10.26	63	14.03	14.23	

ν — stretching, β — in-plane bending, σ — scissoring, δ — rocking, γ — out-of-plane bending, τ — twisting, ω — wagging, s — symmetric, as — antisymmetric. Potential energy distribution (PED) less then 10% are not shown.

3.2.1. C–H vibrations

The heteroaromatic organic compounds commonly exhibit multiple weak bands in the region 3100–3000 cm^{-1}, which is the characteristic region for the ready identification of C–H stretching vibrations and these vibrations are not found to be affected due to the nature and position of the substituent [39, 40]. In the present work, the vibrations (ν 1–4 and ν 5–6) in Table II are assigned to C–H symmetric and asymmetric stretching modes, respectively. The theoretical vibrations due to C–H symmetric and asymmetric stretching wavenumbers were obtained in the range of 3127.98–3108.80 cm^{-1}, 3131.36–3114.18 cm^{-1}, 3203.85–3184.73 cm^{-1} and 3093.60–3059.59 cm^{-1}, 3099.22–3064.99 cm^{-1}, 3171.12–3130.68 cm^{-1} by the B3LYP/6-311++G(d,p), B3PW91/6-311++G(d,p), and BPV86/6-311++G(d,p)

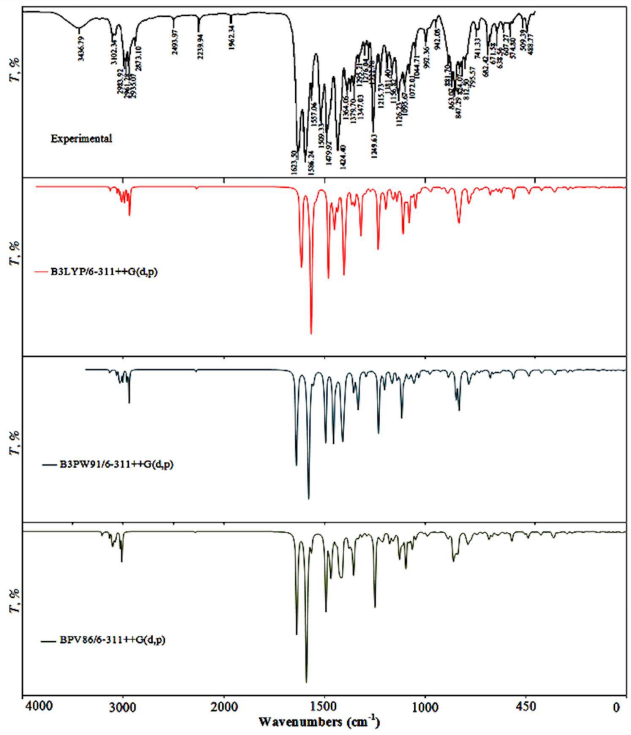

Fig. 3. Experimental and theoretical FT–IR spectra of the title compound.

methods, respectively. Similarly, the experimental FT–IR spectra of the title compound are found at 3436.79 and 3102.34 cm^{-1} [9]. As indicated by PED, these (symmetric and asymmetric) modes are pure stretching modes involving the exact contributions of $> 95\%$. Thus, the aromatic C–H stretching vibrations remain unchanged due to the nature and position of bromine substitution.

The C–H in–plane bending vibrations appear in the region 1500–1100 cm^{-1}, while the C–H out–of–plane vibrations lie in the region 1000–750 cm^{-1} [41, 42]. In the title compound, the calculated C–H in–plane bending vibrations frequencies using the B3LYP, B3PW91, and BPV86 levels with 6-311++G(d,p) basis set (mode nos. 30, 38, 41, 46 and 33, 40, 42) were found to be at 1397.65 (10%), 1401.68 (14%), 1413.10 (12%); 1231.74 (14%), 1231.57 (17%), 1223.49 (24%); 1139.91 (44%), 1137.83 (49%), 1112.16 (43%); 1028.29 (15%), 1031.75 (17%), 1044.36 (30%) cm^{-1} and 1351.92 (12%), 1334.37 (10%), 1356.29 (17%); 1159.82 (18%), 1166.17 (17%), 1156.78 (25%); 1097.23 (31%), 1105.06 (19%), 1095.95 (11%) cm^{-1} for ring1 as 5-bromo-1*H*−indazole and ring2 as 2-cyanopyridine, respectively. The bands observed in the FT–IR spectrum at 1379.70, 1249.63, 1156.82, 1044.71 cm^{-1} and 1347.03, 1181.40, 1126.23 cm^{-1} assigned to in–plane bending vibrations for ring1 and ring2, respectively [9]. In the present work, the C–H out–of–plane bending vibrations were obtained in the range of 933.41–784.05, 930.95–782.53, 930.40–783.45 cm^{-1} (mode nos. 51, 53, and 57) for ring1 and 959.13–828.53, 957.90–829.96, 959.76–791.82 cm^{-1} (mode nos. 49, 54, 55, and 56) for ring2 using the B3LYP/6-311++G(d,p), B3PW91/6-311++G(d,p), and BPV86/6-311++G(d,p) methods, respectively. The FT–IR bands at 942.08, 881.70, 847.29, 824.07, 795.57 cm^{-1} are assigned to C–H out–of–plane bending vibrations of the title compound.

3.2.2. CH_3 and CH_2 Vibrations

The stretching vibrations of CH_2 and CH_3 groups possess the asymmetric and symmetric stretches are expected in the range 300–2900 and 2900–2800 cm^{-1} [43, 44], respectively. The asymmetric stretching modes of the CH_2 and CH_3 groups are usually observed at higher than the symmetric stretching modes [45].

The asymmetric CH_2 and CH_3 groups stretching vibrations are observed at 2983.92 and 2961.28 cm^{-1}, while the symmetric CH_2 and CH_3 groups stretching vibrations are found at 2935.07 cm^{-1} for the title compound in the FT–IR spectrum [9]. The computed values (mode nos. 7–12/13–15) in the region 3035.60–2984.22 / 2956.84–2932.85, 3039.40–3000.57 / 2961.55–2936.85, 3106.05–3069.26 / 3025.13–3007.85 cm^{-1} with the contributions of 32–96 / 93–97, 33–92 / 77–96, 17–90 / 94–99% are designated to asymmetric/symmetric CH_2 and CH_3 groups stretching vibrations using the B3LYP/6-311++G(d,p), B3PW91/6-311++G(d,p), and BPV86/6-311++G(d,p) methods, respectively.

The CH_2 and CH_3 groups in-plane/out-of-plane bending vibrations are fall within the computed wavenumber, as shown in Table II.

3.2.3. C=O Vibrations

The carbonyl (C=O) group stretching frequency appears strongly in the FT–IR spectrum in the range of 1800–1600 cm^{-1} [46] because of the high change in dipole moment. The calculated absorption at 1616.01 (77%), 1639.97 (78%), and 1637.14 cm^{-1} (76%) for the title compound by the B3LYP, B3PW91, and BPV86 levels, respectively, is mode 17 which belongs to the stretching of C=O bond of carboxylic acid diethylamide substituent on the pyrazole ring, respectively Strong FT–IR absorption band at 1623.50 cm^{-1} [9] is assigned to the carbonyl stretching vibration for the title compound.

The C=O in–plane bending vibrations of carboxylic acid diethylamide substituent on the pyrazole ring (mode nos. 72 and 74) are calculated at 447.07, 447.33, 452.54 cm^{-1} and at 417.88, 416.00, 422.99 cm^{-1} which both have the PED values 13%, using the B3LYP, B3PW91, and BPV86 methods, respectively. In the present work, the bands observed at 682.42 cm^{-1} [9] in the FT–IR spectrum and at 771.29, 770.52, 7773.39 cm^{-1} and at 714.33, 714.14, 714.05 cm^{-1} theoretically, using the B3LYP/6-311++G(d,p), B3PW91/6-311++G(d,p), and BPV86/6-311++G(d,p) methods, are assigned as γ (ONCC) carbonyl (C=O) group out–of–plane bending vibrations with PED contributions of 32%.

3.2.4. C–N, C≡N, and N–N Vibrations

The C–N stretching modes are expected in the range 1100–1300 cm^{-1} of the vibrational spectrum, i.e., mixing of several bands are possible in this region [47]. In the study done Sert et al. [48], the bands at 1410, 1387, 1336, 1269, 1206, 1089 cm^{-1} were assigned to C–N stretching vibration in the pyrazole ring. The theoretically computed values of ν(NC) stretching vibrations in pyrazole ring (ring1), 2-cyano-pyridine (ring2), and carboxylic acid diethylamide (mode nos. 30, 36, and 39) are found at 1397.65 (14%) 1273.14 (26%), 1194.95 (32%) cm^{-1} for B3LYP; 1401.68 (13%) 1272.11 (12%), 1202.92 (34%) cm^{-1} for B3PW91; 1413.10 (31%) 1289.03 (12%), 1212.34 (35%) cm^{-1} for BPV86 levels, respectively. The C–N stretching vibrations in pyrazole ring (ring1), 2-cyano-pyridine (ring2) and carboxylic acid diethylamide of the title compound are assigned at 1379.70, 1276.04, and 1215.73 cm^{-1} [9] in the FT–IR spectrum.

For the aromatic compound which bears a cyano group (C≡N) attached to the ring, a band of good intensity in the region 2260–2221 cm^{-1} is assigned to ν (C≡N) stretching vibration [49]. In the case of the title compound the FT–IR band at 2239.94 cm^{-1} was assigned to ν (C≡N) stretching vibration [9]. In the present study, the ν (C≡N) stretching mode (mode no. 16) was calculated at 2268.58, 2276.73, and 2284.36 cm^{-1} using the B3LYP, B3PW91, and BPV86 levels with 90, 89, and 90% to PEDs respectively In plane bending mode of C≡N group is calculated at 558.69, 558.64, and 564.94 cm^{-1} using the B3LYP, B3PW91, and BPV86 levels with the 6-311++G(d,p) basis set, respectively. In out–of–plane bending vibrations of C≡N group (mode nos. 70, 75) are calculated at 483.07, 366.23 cm^{-1} (32 46%) for B3LYP; 482.78, 364.85 cm^{-1} (33 45%) for B3PW91; 487.18, 364.08 cm^{-1} (13, 43%) for BPV86.

Evecen et al. calculated this N–N stretching vibration of the pyrazole ring as 1112 cm^{-1} for the B3LYP/6-311++G(d,p) method [50]. The N–N stretching vibration of the pyrazole ring was calculated at 1206 and 1180 cm^{-1} using the B3LYP/6-311++G(d,p) method by Sert et al. [48]. The experimental ν (N–N) stretching band (mode nos. 4 and 42) of the pyrazole ring was observed at 1181.40 and 1126.23 cm^{-1} in the FT–IR spectrum [9]. The theoretically calculated values were obtained at 1159.82 and 1097.23 cm^{-1} for B3LYP, 1166.17 and 1105.06 cm^{-1} for B3PW91, and 1156.78 and 1095.95 cm^{-1} for BPV86.

3.2.5. C–Br Vibrations

Bromine atom attached to an aromatic ring usually has stretching vibration mode (C–Br) expected in the region 650–450 cm^{-1} [51]. The C–Br stretching mode appears in the region 200–480 cm^{-1} as reported by Varsanyi [52]. In the spectra of the title compound the ν (C–Br) stretching vibration contributes to the bands computed at 331.55, 333.70, and 338.03 cm^{-1} (which is contributing to 22, 21, and 21%, respectively) by the B3LYP/6-311++G(d,p), B3PW91/6-311++G(d,p), and BPV86/6-311++G(d,p) methods (mode 76, in Table II). According to the calculated PED, the in-plane bending σ (BrCC) vibrations in the title compound should be assigned to the band at 251.28, 249.40, 255.44 cm^{-1} and 178.93, 177.37, 182.66 cm^{-1} (which are contributing to almost 19% and 12% respectively) by the B3LYP, B3PW91, and BPV86 methods (modes 80 and 83). The calculated bands at 289.82, 290.54, 293.88 cm^{-1} and 97.83, 97.08, 98.22 cm^{-1} which are contributing to 14, 15, 13% and 15, 16, 17% by the B3LYP/6-311++G(d,p), B3PW91/6-311++G(d,p), and BPV86/6-311++G(d,p) methods (modes 78 and 88) are assigned to C–Br out-of-plane bending vibrations of the title compound, respectively.

3.3. FMOs and Ultraviolet–Visible (UV-Vis) spectral analysis

The frontier molecular orbitals (FMOs) called the highest occupied molecular orbital (HOMO) and the lowest unoccupied molecular orbital (LUMO) are the main orbitals taking part in the electric and optical properties, as well as in the UV Vis spectra [53]. The HOMO (defined as an electron donation) presents the outermost orbital filled by electrons and is directly related to the ionization potential/I, while the LUMO (defined as an electron acceptance) implies the first empty innermost orbital unfilled by electron and is directly related to the electron affinity/A. The 3D orbital pictures of the FMOs obtained at the B3LYP/6-311++G(d,p), B3PW91/6-311++G(d,p), and BPV86/6-311++G(d,p) methods for the title compound are given in Fig. 4. It is evident from Fig. 4, the LUMO spread over the whole molecule except the CH_2 and CH_3 groups and Br atom whereas the region of HOMO spread approximately over the entire molecule except for the cyano group of pyridine ring, H atoms of rings, CH_2 and CH_3 groups by the all of the level of theories.

The density of state (DOS) of a molecule is the number of allowed electrons (or holes) per interval of energy at each energy level to be occupied. We have used GaussSum 2.2 program [54] to calculate the group contributions to the FMOs (HOMO and LUMO) The DOS diagrams obtained at the B3LYP/6-311++G(d,p), B3PW91/6-311++G(d,p), and BPV86/6-311++G(d,p) methods of the title compound are plotted in Fig. 4. The DOS spectrum is a simple view of the character of the molecular orbitals in the energy gap of the molecule resulting from the simultaneous effect of acceptor and donor group and to spacer effect on the electron delocalization (Fig. 4). The green and red line in the DOS spectrum indicates the occupied and virtual orbitals, respectively.

The energy difference between the LUMO and HOMO energies is called as energy gap ($\Delta E_{\mathrm{LUMO-HOMO}}$). The HOMO–LUMO energy gap reveals the chemical reactivity and kinetic stability of the molecule.

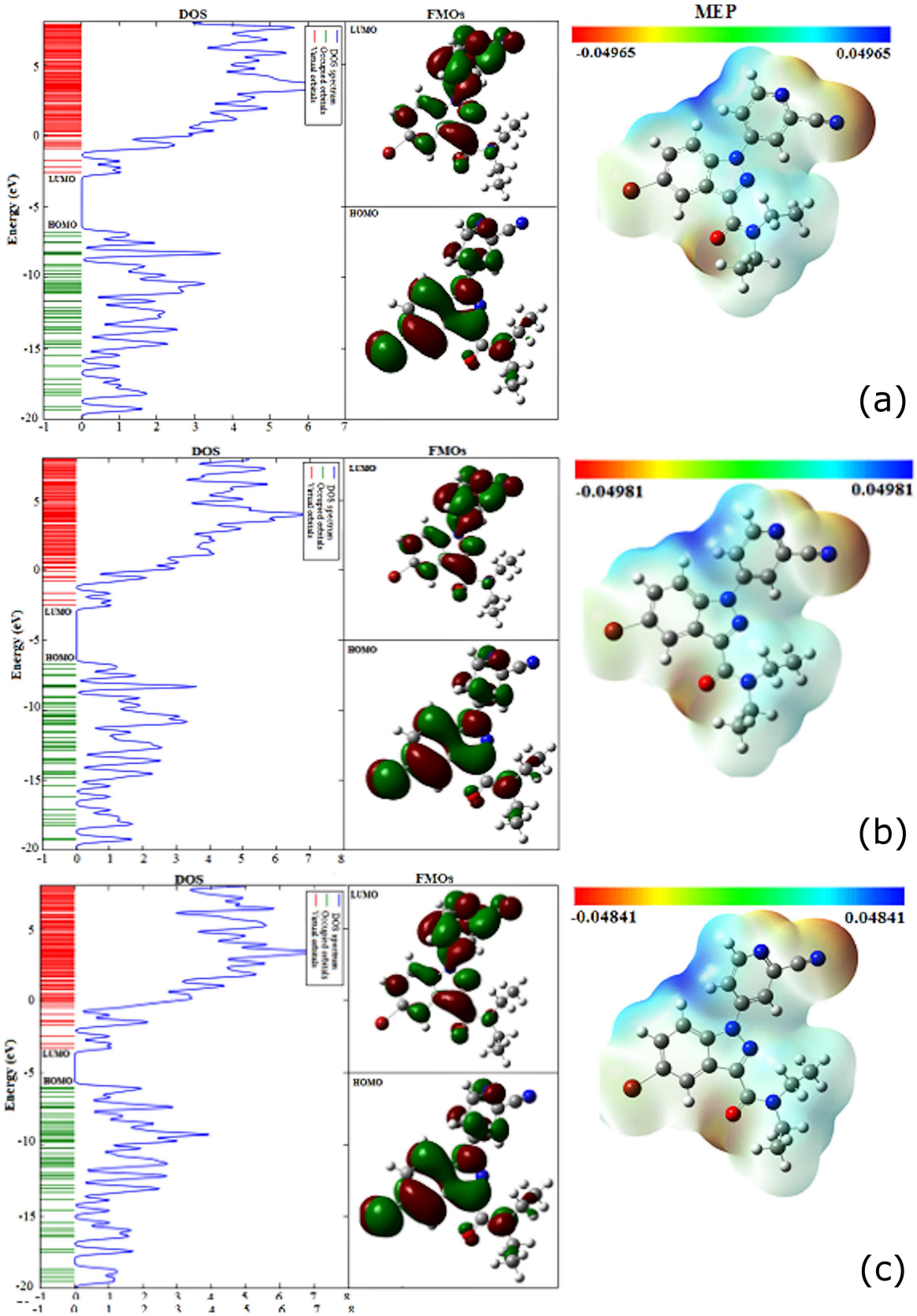

Fig. 4. The DOS, FMOs and 3D plot of the MEP obtained at the (a) B3LYP/6-311++G(d,p), (b) B3PW91/6-311++G(d,p), and (c) BPV86 /6-311++G(d,p) methods for the title compound.

TABLE III

Total energy (in a.u.), E_{HOMO}, E_{LUMO}, $\Delta E_{\mathrm{LUMO-HOMO}}$, ionization potential ($I$), electron affinity ($A$), global hardness ($\eta$), chemical potential ($P_i$), electrophilicity index (ω), (all in eV), and global softness (σ), (in eV^{-1}) values of the title compound using the TD-DFT methods.

	B3LYP/6-311++G(d,p)		B3PW91/6-311++G(d,p)		BPV86/6-311++G(d,p)	
	Gas	Chloroform	Gas	Chloroform	Gas	Chloroform
total energy	−3618.795	−3618.809	−3618.361	−3618.374	−3619.162	−3619.174
E_{HOMO}	−6.833	−6.707	−6.870	−6.759	−6.105	−6.007
E_{LUMO}	−2.580	−2.465	−2.593	−2.494	−3.347	−3.259
$\Delta E_{\mathrm{LUMO-HOMO}}$	4.253	4.242	4.277	4.265	2.758	2.748
I	6.833	6.707	6.870	6.759	6.105	6.007
A	2.580	2.465	2.593	2.494	3.347	3.259
η	2.127	2.121	2.139	2.133	1.379	1.374
σ	0.470	0.471	0.468	0.469	0.362	0.728
P_i	−4.707	−4.586	−4.732	−4.627	−4.726	−4.633
ω	5.208	4.958	5.234	5.019	8.098	7.811

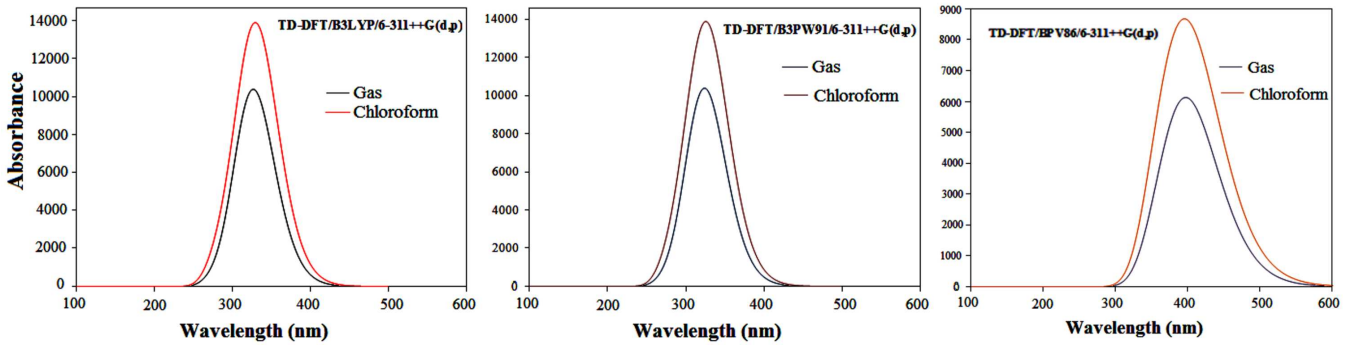

Fig. 5. The UV-Vis absorption spectrum in the gas phase and chloroform solvent of the title compound by TD-DFT/B3LYP, TD-DFT/B3PW91, and TD-DFT/BPV86 methods with 6-311++G(d,p) basis set.

The decrease in the value of $\Delta E_{\mathrm{LUMO-HOMO}}$ indicates strong molecular interaction within the molecule due to intramolecular charge transfer (ICT) from donor to acceptor atom. The total energy, HOMO and LUMO energies, and the $\Delta E_{\mathrm{LUMO-HOMO}}$ energy gap calculations in the chloroform solvent and gas phase were performed by time-dependent density functional theory (TD-DFT) and the values are presented in Table III. The energy gap values are found to be 4.253, 4.277, 2.758 eV in the gas phase and 4.242, 4.265, 2.748 eV in the chloroform solvent obtained at B3LYP/6-311++G(d,p), B3PW91/6-311++G(d,p), and BPV86/6-311++G(d,p) methods of the title compound, respectively. By the three DFT-functionals, the $\Delta E_{\mathrm{LUMO-HOMO}}$ energy gaps in the gas phase and chloroform solvent are both decreased in the order: B3PW91 > B3LYP > BPV86. The TD-DFT/BPV86 method in the gas phase and chloroform solvent has the lowest energy gap values compared to those calculated by the B3PW91, B3LYP levels. Moreover, lower values in the energy gap of the HOMO-LUMO explain the eventual charge transfer interaction within the molecule. For the title compound, the $\Delta E_{\mathrm{LUMO-HOMO}}$ values decrease as the phase changes from gas to solvent. According to the results, the title compound in the gas phase is more stable than in the solution phase.

The UV-Visible spectral analyses of the title compound has been investigated by the theoretical calculations. The time dependent DFT (TD-DFT) calculations at the B3LYP, B3PW91, and BPV86 levels on electronic absorption spectra have been used to find out the absorption wavelengths (λ, nm), excitation energies (E, eV) oscillator strengths (f), and major orbital transitions of the title compound for the gas phase molecule as well as in chloroform solvent. The oscillator strengths, absorption wavelengths, excitation energies, their assignments, and contributions were calculated using the TD-DFT/B3LYP, TD-DFT/B3PW91, and TD-DFT/BPV86 methods with the 6-311++G(d,p) basis set with chloroform solvent and the gas phase are given in Table IV. The major contributions of the HOMO–LUMO transitions were calculated using the Gauss-Sum 2.2 program [54] based on the obtained TD-DFT results. The simulated absorption spectrum of the title compound was carried out in various methods with the chloroform solvent and gas phase and these results are presented in Fig. 5.

TABLE IV

Calculation UV?Vis spectra of the title compound using the TD-DFT/B3LYP, TD-DFT/B3PW91, and TD-DFT/BPV86 methods with the 6-311++G(d,p) basis set in gas phase and chloroform solvent (H→L — HOMO→LUMO).

Methods	Transition	%		λ [nm]	E [eV]	f [a.u]
B3LYP/6-311++G(d,p)	H→L	96	Gas	329.73	3.7601	0.2196
		97	Chloroform	333.79	3.7144	0.2914
	H −1 →L	84	Gas	312.28	3.9703	0.0172
		57	Chloroform	306.93	4.0394	0.0463
	H→L + 1	88	Gas	307.25	4.0353	0.0293
		61	Chloroform	310.01	3.9993	0.0338
	H −1 →L + 1	88	Gas	285.24	4.3466	0.0045
		55	Chloroform	284.63	4.3559	0.0194
B3PW91/6-311++G(d,p)	H→L	96	Gas	327.53	3.7854	0.2138
		97	Chloroform	331.55	3.7395	0.2817
	H −1 →L	87	Gas	312.28	3.9703	0.0191
		73	Chloroform	309.24	4.0093	0.0222
	H→L + 1	90	Gas	305.13	4.0633	0.0365
		75	Chloroform	305.46	4.0589	0.0696
	H −1 →L + 1	90	Gas	285.46	4.3433	0.0042
		77	Chloroform	284.19	4.3627	0.0127
BPV86/6-311++G(d,p)	H→L	92	Gas	439.63	2.8202	0.0027
		85	Chloroform	440.94	2.8118	0.0137
	H −1 →L	61	Gas	414.82	2.9889	0.0586
		78	Chloroform	413.08	3.0014	0.1145
	H→L + 1	90	Gas	396.02	3.1307	0.0056
		83	Chloroform	391.30	3.1685	0.0233
	H −1 →L + 1	62	Gas	379.69	3.2654	0.0418
		69	Chloroform	371.68	3.3357	0.0809

The maximum calculated absorption spectra of the title compound consists of an intense transition band (by TD-DFT with the B3LYP / B3PW91 / BPV86 levels) at 329.73 / 327.53 / 439.63 and 333.79 / 331.55 / 440.94 nm (3.7601 / 3.7854 / 2.8202 eV and 3.7144 / 3.7395 / 2.8118 eV) with oscillation strength values of 0.2196 / 0.2138 / 0.0027 and 0.2914 / 0.2817 / 0.0137 in the gas and chloroform, respectively. These transitions in the gas and chloroform correspond to 99 / 96 / 92% and 97 / 97 / 85% contributions from HOMO to LUMO orbital ($\pi \rightarrow \pi*$ transitions) for with a charge transfer (CT) character from electron-donor to electron-acceptor, respectively.

3.4. Molecular electrostatic potential (MEP) analysis

The molecular charge distribution was represented by the map of molecular electrostatic potential (MEP) which helps in predicting the sites for the nucleophilic and electrophilic attack in the molecule. The negative (red, orange, and yellow) regions of the MEP are related to the electrophilic reactivity and the positive (blue color) ones belong to the nucleophilic reactivity. The 3D plots of molecular electrostatic potential calculated at the B3LYP, B3PW91, and BPV86 methods for the title compound are shown in Fig. 4. The color code maps of the title compound are predicted in between −0.04965, −0.04981, and −0.04841 a.u (deepest red) and 0.04965, 0.04981, and 0.04841 a.u (deepest blue) for the B3LYP, B3PW91, and BPV86 methods, respectively. As can be seen in Fig. 4, the region of negative charge is displayed in red color and it is found around the electronegative oxygen and Br atoms, N atom of cyano group, and N atom of pyridine ring in the title compound for the B3LYP, B3PW91, and BPV86 methods. The red color region is susceptible to electrophilic attack. The MEP maps of the studied molecule clearly show that the maximum positive potential region (blue) is localized on the hydrogen atoms. The blue color region represents a strong positive region and is prone to nucleophilic attack.

3.5. Global Reactivity Descriptors

According to Koopmans' theorem [55], a detailed investigation of quantum molecular descriptors of the title compound using the TD-DFT/B3LYP, TD-DFT/B3PW91, and TD-DFT/BPV86 methods with the 6-311++G(d,p) basis set with the chloroform solvent and gas phase such as ionization potential ($I = -E_{\mathrm{HOMO}}$), electron affinity ($A = -E_{\mathrm{LUMO}}$), global hardness ($\eta = (I - A)/2$), chemical potential

($P_i = -(I + A)/2$), electrophilicity index ($\omega = P_i^2/2\eta$), and global softness ($\sigma = P_i/(2\eta)$) was calculated and listed in Table III. The global hardness (η) and global softness (σ) correspond to the energy gap between the E_{LUMO} and E_{HOMO} energies have been associated with the stability of the chemical system. A molecule with a small energy gap has high chemical reactivity than a hard one because it could easily offer electrons to an acceptor [56]. The values of η/σ of the title compound are found to be 2.127/0.470, 2.139/0.468, 1.379/0.362 and 2.121/0.471, 2.133/0.469, 1.374/0.728 in the gas phase and chloroform solvent obtained with the TD-DFT/B3LYP, TD-DFT/B3PW91, and TD-DFT/BPV86 methods, respectively. As can be seen from the results the global hardness/softness values of the studied molecule decrease/increase when solvent is taken into account. The results of large η and $\Delta E_{\mathrm{LUMO-HOMO}}$ values obtained by the TD-DFT methods also support the stability of the title molecule in gas phase.

3.6. Mulliken and natural population analyses

The atomic charges have an important role in the application of quantum chemical calculations of a molecular system due to change in dipole moment, polarizability, electronic structure, vibrational spectra, and more properties for a molecular system [57]. Our interest here is the comparison of different methods to describe the electron distribution of the title compound. The atomic charge values obtained by Mulliken and Natural bond orbital (NBO) analysis for the title compound calculated with the B3LYP, B3PW91, and BPV86 levels with the 6-311++G(d,p) basis set are listed in Table V. The represented graphical form of the results is shown in Fig. 6. The change in the charge distribution in Fig. 6 shows a response to using a broad variety of methods (B3LYP, B3PW91, and BPV86).

According to the Mulliken and NBO methods, the N3, N5, O1 atoms have negative atomic charges $-0.063e$ and $-0.263e$ / $-0.174e$ and $-0.289e$ / $-0.287e$ and $-0.641e$ for the B3LYP level, -0.020e and -0.272e / $-0.175e$ and $-0.290e$ / $-0.267e$ and $-0.641e$ for the B3PW91 level, and $-0.117e$ and $-0.266e$ / $-0.146e$ and $-0.281e$ / $-0.256e$ and $-0.615e$ for the BPV86 level. The results are in good agreement with each other and with MEP results.

According to Mulliken and NBO charge's plot (Fig. 6) all of the hydrogen atoms have net positive charges. In the title compound, the H8 atom in the 5-bromo-1H-indazole has the highest positive charge calculated at the B3LYP, B3PW91, and BPV86 levels with the 6-311++G(d,p) basis set compared with other hydrogen atoms due to the electron-withdrawing nature of the O1 atom. The O1 and N3 display strong electronegativity, the theoretical Mulliken and NBO atomic charges of H8 / H3a found to be 0.283e and 0.258e/0.213e and 0.215e for the B3LYP level, 0.324e and 0.214e/0.252e and 0.193e for the B3PW91 level, and 0.285e and 0.216e/0.230e and 0.199e for the BPV86 level exhibited the largest positive charges, respectively. As can be seen for RDG results, this is due to the presence of strong intramolecular hydrogen bonds and steric interactions between O1$\cdots$H8 and N3$\cdots$H3a.

While the C18 and Br1 atomic charges derived from Mulliken are negative, the NBO atomic charges indicate positive values. Figure 6 shows that the NBO atomic charges are more reliable to the differences in the molecular systems than Mulliken's net charges.

TABLE V

Comparative of Mulliken and NBO atomic charges of the title compound obtained by the B3LYP, B3PW91, and BPV86 levels with the 6-311++G(d,p) basis set.

Atoms	B3LYP		B3PW91		BPV86	
	Mulliken	NBO	Mulliken	NBO	Mulliken	NBO
C1	−0.413	−0.585	−0.505	−0.556	−0.457	−0.569
C2	−0.185	−0.173	−0.258	−0.138	−0.230	−0.153
C3	−0.305	−0.172	−0.374	−0.128	−0.358	−0.152
C4	−0.478	−0.581	−0.612	−0.558	−0.519	−0.567
C5	−0.546	0.652	−0.729	0.634	−0.755	0.598
C6	−0.244	0.125	−0.271	0.135	−0.187	0.119
C7	0.773	−0.080	0.880	−0.092	0.810	−0.069
C8	−0.400	−0.170	−0.487	−0.142	−0.450	−0.153
C9	0.081	−0.126	0.016	−0.119	0.044	−0.099
C10	−0.566	−0.184	−0.759	−0.206	−0.714	−0.192
C11	−0.179	−0.228	−0.172	0.656	−0.197	−0.638
C12	0.276	0.162	0.256	−0.238	0.323	0.148
C13	−0.262	0.202	−0.261	0.226	−0.313	0.212
C14	0.250	−0.252	0.313	−0.233	0.366	−0.228
C15	−0.104	0.078	−0.177	0.106	−0.216	0.093
C16	0.503	0.084	0.473	0.113	0.359	0.103
C17	0.340	−0.195	0.391	−0.199	0.439	−0.196
C18	−1.385	0.280	−1.616	0.272	−1.461	0.265
N1	0.135	−0.486	0.286	−0.449	0.240	−0.423
N2	0.559	−0.224	0.705	−0.237	0.705	−0.200
N3	−0.063	−0.263	−0.020	−0.272	−0.117	−0.266
N4	0.056	−0.421	0.118	−0.413	0.128	−0.402
N5	−0.174	−0.289	−0.175	−0.290	−0.146	−0.281
O1	−0.287	−0.641	−0.267	−0.641	−0.256	−0.615
Br1	−0.176	0.076	−0.243	0.081	−0.194	0.088
H1a	0.182	0.214	0.207	0.204	0.196	0.200
H1b	0.148	0.205	0.173	0.193	0.165	0.198
H1c	0.125	0.192	0.144	0.182	0.136	0.187
H2a	0.200	0.223	0.230	0.198	0.214	0.202
H2b	0.138	0.188	0.166	0.173	0.152	0.178
H3a	0.213	0.215	0.252	0.193	0.230	0.199
H3b	0.157	0.189	0.191	0.173	0.178	0.179
H4a	0.178	0.207	0.210	0.197	0.196	0.201
H4b	0.150	0.206	0.173	0.194	0.165	0.199
H4c	0.129	0.197	0.149	0.187	0.139	0.191
H8	0.283	0.258	0.324	0.214	0.285	0.216
H10	0.234	0.228	0.279	0.178	0.248	0.195
H11	0.154	0.219	0.193	0.327	0.160	0.179
H14	0.195	0.224	0.236	0.184	0.201	0.187
H15	0.207	0.197	0.248	0.162	0.226	0.164
H17	0.262	0.250	0.314	0.215	0.265	0.217

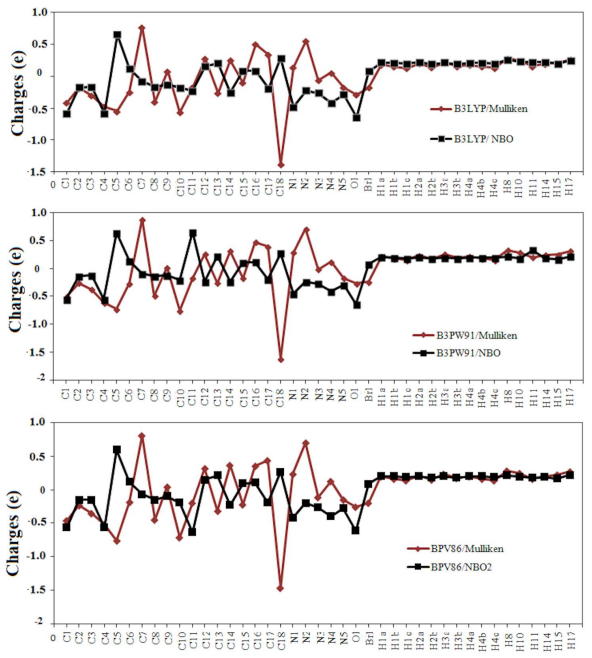

Fig. 6. Histogram of Mulliken and NBO atomic charges using the B3LYP, B3PW91, and BPV86 levels with the 6-311++G(d,p) basis set of the title compound.

3.7. ^1H and ^{13}C NMR calculations

Nuclear magnetic resonance (NMR) spectroscopy is a useful tool for determinations of molecular structures of organic molecules developed during the last 40 years [58]. The chemical shifts of ^{1}H and ^{13}C NMR of C and H were calculated using the gauge-independent atomic orbital (GIAO) method with respect to tetramethylsilane (TMS), in the investigated gas phase, chloroform solvent and compared with experimental ^{1}H and ^{13}C chemical shift values [9]. The ^{1}H and ^{13}C spectrum of the tetramethylsilane (TMS) molecule was calculated using the same methods used as a reference. The ^{1}H and ^{13}C chemical shift values were converted to the TMS scale by subtracting the calculated absolute chemical shielding of TMS which are calculated at the same levels ($\delta^x_{\mathrm{rel}} = \delta^{\mathrm{TMS}}_{\mathrm{abc}} - \delta^x_{\mathrm{abc}}$, where δ^x_{rel} is the chemical shift, δ^x_{abc} is the absolute shielding and $\delta^{\mathrm{TMS}}_{\mathrm{abc}}$is the absolute shielding of TMS). The experimental [9] and theoretical ^{1}H and ^{13}C chemical shifts calculated at the B3LYP, B3PW91, and BPV86 levels with the 6-311++G(d,p) basis set in the gas phase and chloroform solvent for the title compound are tabulated in Table VI. The atoms of the title compound were numbered according to Fig. 1.

The chemical shift of C5 for the title compound shows the maximum value (161.24 ppm) among the other carbon atoms experimentally [9] and computed (167.20/168.55, 165.08/166.37, and 161.59/162.79 ppm) bigger than the other carbon chemical shifts theoretically using the B3LYP, B3PW91, and BPV86 levels with the 6-311++G(d,p) basis set in the gas/chloroform, respectively. This supports the high positive charges (0.652, 0.634, and 0.598) prediction by NBO obtained with the B3LYP, B3PW91, and BPV86 levels of the title compound, which is mainly due to the O atom attached to this carbon atom. The chemical shift values of C1, C4 and C2, C3 are smaller than the other aromatic carbons because of the substitution of methyl and methylene groups. The ^{13}C NMR spectrum having methyl (CH_3) and methylene (CH_2) signals show that the peaks of CH_3 carbons are smaller than those of CH_2 carbon atoms. From the ^{13}C NMR spectrum, the signals of the CH_2 (C2, C3) and CH_3 (C1, C4) group of the title compound are observed at 41.11, 43.37 and 12.75, 14.72 ppm. The computed values are shown in the same parallel as seen in Table VI. The computed and recorded results are in very good agreement for similar structures [59]. The computed chemical shift of the C atom in the cyano group using the B3LYP, B3PW91, and BPV86 levels of the title compound was 122.28/124.87, 123.19/125.68, and 121.73/124.09 ppm in gas phase/chloroform solvent and the corresponding experimental value is 116.64 ppm, respectively.

The values of the chemical shift for hydrogen atoms which are attached with benzene ring are in the interval between 7 and 8 ppm [60]. For 2-styrylpyrydine, *IIIa* and *IIIc*, the chemical shift for H atom (H3) in the pyridine ring was calculated at 8.9 ppm using the B3LYP/6-311++G(d,p) in both gas phase and $CDCl_3$ solvent [61]. There are three H atoms in the pyridine ring whose values are 7.93, 8.82, 8.42 ppm experimentally [9], the corresponding theoretical values using the B3LYP, B3PW91, and BPV86 levels of the title compound lie between 7.80–8.95/8.12–9.06, 7.88–9.00/8.20–9.11, and 7.71–8.85/8.02–8.95 ppm in gas phase/chloroform solvent, respectively. These values in the pyridine ring are closer to the expected values for hydrogen atoms which are attached with benzene ring. The six H atoms of the two methyl groups give signals to 1.26 and 1.37 ppm experimentally [9], while the calculated values using the B3LYP, B3PW91, BPV86 levels of the title compound are in the range 1.02–1.74/1.09–1.61, 1.00–1.73/1.06–1.60, 1.01–1.60/1.08–1.48 ppm and 1.18–1.86/1.22–1.85, 1.12–1.86/1.16–1.83, 1.22–1.78/1.25–1.75 ppm in gas phase/chloroform solvent, respectively. This is in agreement with the literature value [62]. When the chemical shifts in the gas phase and chloroform solvent are compared, there is no appreciable difference observed in the chemical shifts. Hence, the effect of the solvent on the chemical shifts of various atoms for the title compound is negligibly small.

3.8. Nonlinear Optical (NLO) Properties

Nonlinear optical (NLO) materials have been extensively researched due to their potential applications in the field of optoelectronic such as optical communication, optical computing, optical switching, optical modulation, optical logic, and dynamic image processing [63].

TABLE VI

Theoretical and experimental [9] ^{1}H and ^{13}C isotropic chemical shifts (with respect to TMS, all values in ppm) in gas phase and chloroform solvent for the title compound.

Atoms	Calculated						Exp. [9]
	B3LYP/6-311++G(d.p)		B3PW91/6-311++G(d.p)		BPV86/6-311++G(d.p)		
	Gas	Chloroform	Gas	Chloroform	Gas	Chloroform	
H1a	1.74	1.61	1.73	1.60	1.60	1.48	1.26
H1b	1.02	1.09	1.00	1.06	1.01	1.08	1.26
H1c	1.10	1.20	1.09	1.18	1.07	1.16	1.26
H2a	4.44	4.35	4.44	4.34	4.58	4.47	3.79
H2b	2.84	3.01	2.85	3.00	2.88	3.03	3.61
H3a	4.37	4.40	4.32	4.33	4.67	4.67	3.74
H3b	3.11	3.23	3.09	3.21	3.25	3.36	3.66
H4a	1.86	1.85	1.86	1.83	1.78	1.75	1.37
H4b	1.18	1.22	1.12	1.16	1.22	1.25	1.37
H4c	1.57	1.61	1.54	1.58	1.54	1.58	1.37
H8	9.27	9.15	9.28	9.16	9.21	9.10	8.13
H10	7.73	7.85	7.79	7.91	7.59	7.71	7.74
H11	7.80	8.06	7.88	8.13	7.76	8.00	7.64
H14	7.80	8.12	7.88	8.20	7.71	8.02	7.93
H15	8.95	9.06	9.00	9.11	8.85	8.95	8.82
H17	8.41	8.60	8.45	8.63	8.35	8.52	8.42
C1	12.89	13.23	12.58	12.92	12.61	12.98	12.75
C2	45.44	45.96	43.78	44.30	45.49	46.08	41.11
C3	46.50	47.15	45.31	45.94	46.96	47.68	43.37
C4	16.23	16.40	15.96	16.13	15.55	15.75	14.72
C5	167.20	168.55	165.08	166.37	161.59	162.79	161.24
C6	149.86	150.10	147.62	147.84	145.11	145.54	143.09
C7	136.95	137.10	135.26	135.37	134.96	135.15	128.07
C8	137.07	136.06	135.78	134.81	133.62	132.68	132.27
C9	144.24	143.42	141.19	140.43	142.81	142.09	117.04
C10	138.28	138.96	137.30	138.03	134.15	135.01	111.64
C11	114.52	116.94	113.89	116.30	112.14	114.53	126.48
C12	144.70	145.89	142.30	143.46	140.18	141.37	137.49
C13	154.77	155.72	152.82	153.74	150.00	150.98	147.08
C14	120.30	123.50	119.70	122.86	117.13	120.32	119.53
C15	158.43	159.73	157.40	158.75	155.64	157.00	152.44
C16	144.17	142.65	142.64	141.19	140.57	139.29	135.37
C17	128.93	131.12	128.25	130.38	126.20	128.43	117.52
C18	122.28	124.87	123.19	125.68	121.73	124.09	116.64

In order to investigate the effects of the B3LYP, B3PW91, and BPV86 levels on the NLO properties of the studied compound, the dipole moments (μ), the polarizabilities (α), the anisotropy of the polarizabilities ($\langle\Delta\alpha\rangle$), and the mean first-order hyperpolarizabilities (β) of the title compound were calculated using the finite-field approach and are presented in Table VII. The mean first-order hyperpolarizability is a third-rank tensor that can be described by a $3 \times 3 \times 3$ matrix. The 27 components of the 3D matrix can be reduced to 10 components due to Kleinman symmetry [64].

The μ, $\langle\alpha\rangle$, $\langle\Delta\alpha\rangle$, and β values using the Cartesian coordinates are given as follows [65]:

$$\mu = \left(\mu_x^2 + \mu_y^2 + \mu_z^2\right)^{1/2}, \tag{3}$$

$$\langle\alpha\rangle = \left(\alpha_{xx} + \alpha_{yy} + \alpha_{zz}\right)/3, \tag{4}$$

$$\langle\Delta\alpha\rangle = \frac{\sqrt{2}}{2}\Big[\left(\alpha_{xx} - \alpha_{yy}\right)^2 + \left(\alpha_{yy} - \alpha_{zz}\right)^2 + \left(\alpha_{zz} - \alpha_{xx}\right)^2 + 6\left(\alpha_{xy}^2 + \alpha_{xz}^2 + \alpha_{yz}^2\right)^2\Big]^{1/2}, \tag{5}$$

$$\beta = \Big[\left(\beta_{xxx} + \beta_{xyy} + \beta_{xzz}\right)^2 + \left(\beta_{yyy} + \beta_{yzz} + \beta_{yxx}\right)^2 + \left(\beta_{zzz} + \beta_{zxx} + \beta_{zyy}\right)^2\Big]^{1/2}. \tag{6}$$

TABLE VII

Dipole moment μ (in D), mean polarizability $\langle\alpha\rangle$ (in a.u. and esu), the anisotropic of the polarizability $\langle\Delta\alpha\rangle$ (in a.u.) and the mean first-order hyperpolarizability β (in a.u. and esu) values obtained using the B3LYP/6-311++G(d,p), B3PW91/6-311++G(d,p), and BPV86/6-311++G(d,p) methods in gas phase.

Parameters	B3LYP	B3PW91	BPV86
μ [D]	4.2592	4.4089	4.1551
$\langle\alpha\rangle$ [a.u.]	288.3068	284.6878	306.4107
$\langle\alpha\rangle\times10^{-24}$ [esu]	42.7271	42.1907	45.4101
$\langle\Delta\alpha\rangle$ [a.u.]	205.5657	202.0617	228.8948
$\langle\Delta\alpha\rangle\times10^{-24}$ [esu]	30.4648	29.9455	33.9222
β [a.u]	1774.7952	1810.8563	3031.1104
$\beta_{\rm tot}\times10^{-30}$ [esu]	15.3330	15.6445	26.1867
$\beta_{\rm tot}/\beta_{\rm urea}$	41	42	70

To have polarizability and mean first-order hyperpolarizability tensors (α_{xx}, α_{xy}, α_{yy}, α_{xz}, α_{yz}, α_{zz} and β_{xxx}, β_{xxy}, β_{xyy}, β_{yyy}, β_{xxz}, β_{xyz}, β_{yyz}, β_{xzz}, β_{yzz}, β_{zzz}) are utilized a frequency job of GAUSSIAN-09W output [10]. The polarizability and the mean first-order hyperpolarizability values of the Gaussian output are given as atomic units (a.u.), but they have been changed into electronic units (esu) by the following factors: 1 a.u. $= 0.1482\times10^{-24}$ esu for α, 1 a.u. $= 8.6393\times10^{-33}$ esu for β [66].

In this study the mean first-order hyperpolarizability (β) values were calculated at 15.3330×10^{-30}, 15.6445×10^{-30}, and 26.1867×10^{-30} esu using the B3LYP, B3PW91, and BPV86 levels with the 6-311++G(d,p) basis set, respectively. The decreasing order of the β is BPV86 > B3PW91 > B3LYP. As seen in Table III, the energy gaps between the HOMO and LUMO orbitals of the title compound are decreased in the order: B3LYP (4.253 eV) > B3PW91 (4.277 eV) > BPV86 (2.758 eV). As expected, the lower is the HOMO–LUMO energy gap the larger is the β value [67]. Urea is one of the standard molecules used in the study of the nonlinear optical (NLO) properties of molecular systems and is thus frequently used as a threshold value for comparative studies [68]. The calculated mean first-order hyperpolarizability values using the B3LYP, B3PW91 and BPV86 levels for the title compound are about 41, 55, and 70 times greater than that of the standard NLO material urea (0.3728×10^{-30} esu). This large hyperpolarizability value of the title compound indicates that it has considerable NLO properties. The obtained results are evidence for the fact that the title compound can be subjected to future studies to probe its NLO properties.

3.9. Reduced Density Gradient (RDG) analysis

Reduced density gradient (RDG) as a dimensionless quantity is used to explore weak interactions in real space based on the electron density and its derivatives [69]. The RDG is given by the equation

$$\mathrm{RDG}(r) = \frac{1}{2\left(3\pi r^2\right)^{1/3}}\,\frac{|\nabla\rho(r)|}{\rho(r)^{4/3}} \tag{7}$$

where $\rho(r)$ is electron density and $\nabla\rho(r)$ is the gradient of $\rho(r)$ at the point $\boldsymbol{r}$. The plot of $\rho(r)$ against sign λ_2 give the information about the nature and strength of the interactions which are measured in terms of the value of density at low gradient spikes. The large and negative values of sgn $(\lambda_2)\rho$ are indicative of stronger attractive interactions (such as dipole–dipole or hydrogen bonding), while positive ones are indicative of strong repulsion interactions. Values near zero indicate very weak Van der Waals interactions. The sign of λ_2, the second greatest eigenvalue of the Hessian matrix of the $\rho(r)$, is used to discriminate bonded ($\lambda_2 < 0$) from non-bonded ($\lambda_2 < 0$) interactions [69]. λ_2 is typically negative (positive) for attractive (repulsive) interactions.

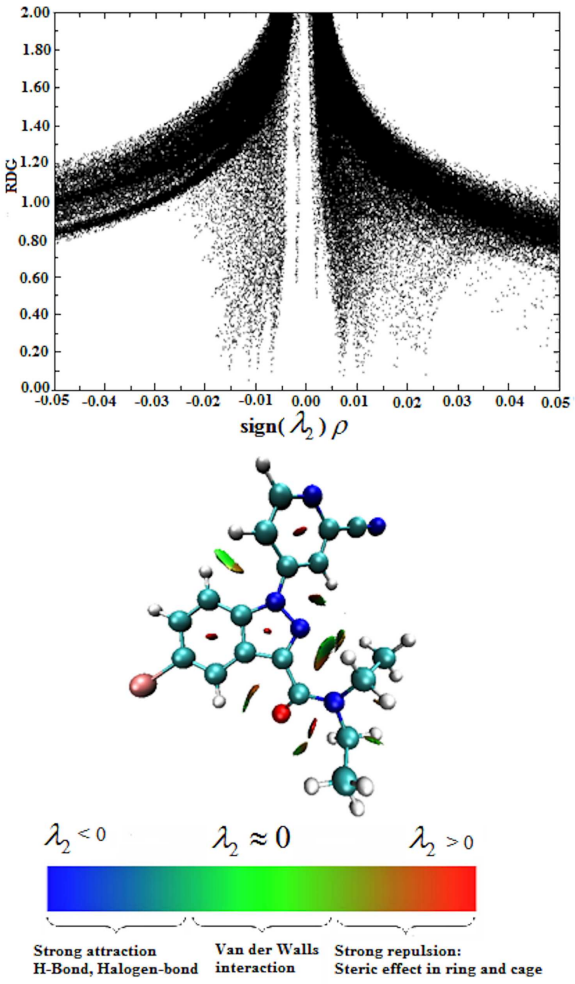

Fig. 7. The reduced density gradient diagram of the title compound using the B3LYP/6-311++G(d,p) level.

The 3D RDG isosurfaces of the title compound are shown in Fig. 7. The software utilized for plotting RDG isosurface is Multiwfn software [26] and it was plotted by VMD program [27]. The RDG analysis was drawn with an isosurface value of 0.5 as illustrated in Fig. 7.

From the RDG isosurface in Fig. 7, the interactions of the region marked by red reflect a strong repulsion (steric effect) in all centers of the ring systems. The color from blue to red indicates from stronger attraction to repulsion, respectively. Within the indazole and pyridine rings for the title compound, the strong steric effect is indicated by red color. The green with slight brown circles can be identified as Van der Waals (VDW) weak attractive interaction due to hydrogen-hydrogen interaction.

4. Conclusions

The detailed interpretations of the molecular structure, vibrational harmonic frequencies, PED assignments, NLO, NMR, Mulliken, and natural bond orbital (NBO) analysis of the title compound were presented using the B3LYP, B3PW91, and BPV86 levels with the 6-311++G(d,p) basis set in this paper. The theoretical geometrical parameters and vibrational frequencies with the PED contributions of the title compound were computed by the B3LYP, B3PW91, and BPV86 calculations with a good accuracy when compared with experimental analysis. In order to understand electronic transitions and quantum descriptors of the title compound, TD-DFT calculations on electronic absorption spectra in the gas phase and chloroform solvent were performed. The lower values of HOMO-LUMO energy gap explain the presence of NLO effect and biological activity of the title compound. The NBO charge distribution study shows the presence of strong intramolecular hydrogen bonds and steric interactions between O1$\cdots$H8 with the maximum negative and positive charges, respectively. The reduced density gradient (RDG) approach was implemented to analyze the weak attractive interactions, strong attraction, and steric repulsion existed in the title compound.

References

[1] K. McClay, S. Mehboob, J. Yu, B.D. Santarsiero, J. Deng, J.L. Cook, H. Jeong, M.E. Johnson, R.J. Steffan, *AMB Express* **5**, 1 (2015).

[2] E. El-Sawy, F. Bassyouni, S. Abu-Bakr, H. Rady, M. Abdlla, *Acta Pharm* **60**, 55 (2010).

[3] M.Z. Zhang, Q. Chen, G-Fu Yang, *Eur. J. Med. Chem.* **89**, 421 (2015).

[4] A. Monge, I. Aldana, T. Alvarez, M.J. Losa, M. Font, E. Cenarruzabeitia, B. Lasheras, D. Frechilla, E. Castiella, E. Fernandez-Alvarez, *Eur. J. Med. Chem.* **26**, 655 (1991).

[5] A. Farghaly, *Arkivoc* **11**, 177 (2010).

[6] T. Chandra, N. Garg, A. Kumar, *Int. J. Chem. Tech. Res.* **2**, 762 (2010).

[7] P. Lissoni, S. Pittalis, F. Rovelli, S. Zecchini, M. Casati, M. Tremolada, F. Pelizzoni, *J. Biol. Regul. Homeost. Agents* **10**, 27 (1996).

[8] K.W. Woods, J.P. Fischer, A. Claiborne, T. Li, S.A. Thomas, G.D Zhu, R.B Diebold, X. Liu, Y. Shi, V. Klinghofer, E.K Han, R. Guan, S.R Magnone, E.F. Johnson, J.J. Bouska, A.M. Olson, R.D Jong, T. Oltersdorf, Y. Luo, S.H. Rosenberg, V.L. Girandaa, Q. Li, *Bioorg. Med. Chem.* **14**, 6832 (2006).

[9] G. Anuradha, G. Vasuki, G. Surendrareddy, A. Veerareddy, P.K. Dubey, *Crystallography Reports* **59**, 527 (2014).

[10] M.J. Frisch, G.W. Trucks, H.B. Schlegel, G.E. Suzerain, M.A. Robb, J.R. Cheeseman Jr., J.A. Montgomery, T. Vreven, K.N. Kudin, J.C. Burant, J.M. Millam, S.S. Iyengar, J. Tomasi, V. Barone, B. Mennucci, M. Cossi, G. Scalmani, N. Rega, G.A. Petersson, H. Nakatsuji, M. Hada, M. Ehara, K. Toyota, R. Fukuda, J. Hasegawa, M. Ishida, T. Nakajima, Y. Honda, O. Kitao, H. Nakai, M. Klene, X. Li, J.E. Knox, H.P. Hratchian, J.B. Cross, V. Bakken, C. Adamo, J. Jaramillo, R. Gomperts, R.E. Stratmann, O. Yazyev, A.J. Austin, R. Cammi, C. Pomelli, J.W. Ochterski, P.Y. Ayala, K. Morokuma, G.A. Voth, P. Salvador, J.J. Dannenberg, V.G. Zakrzewski, S. Dapprich, A.D. Daniels, M.C. Strain, O. Farkas, D.K. Malick, A.D. Rabuck, K. Raghavachari, J.B. Foresman, J.V. Ortiz, Q. Cui, A.G. Baboul, S. Clifford, J. Cioslowski, B. Stefanov, G. Liu, A. Liashenko, P. Piskorz, I. Komaromi, R.L. Martin, D.J. Fox, T. Keith, M.A. Al-Laham, C.Y. Peng, A. Nanayakkara, M. Challacombe, P.M.W. Gill, B. Johnson, W. Chen, M.W. Wong, C. Gonzalez, J.A. Pople, Gaussian 09 (now Gaussian 16), Gaussian Inc., Wallingford (CT) 2016.

[11] T. Keith, J. Millam, GaussView, Version 5.0.9, Semichem. Inc., Shawnee Mission KS, (2009).

[12] A.D. Becke, *J. Chem. Phys.* **98**, 5648 (1993).

[13] C. Lee, W. Yang, R.G. Parr, *Phys. Rev. B* **37**, 785 (1988).

[14] A.D. Becke, *Phys. Rev. A* **38**, 3098 (1988).

[15] J.P. Perdew, J.A. Chevary, S.H. Vosko, K.A. Jackson, M.R. Pederson, D.J. Singh, C. Fiolhais, *Phys. Rev. B* **48**, 4978 (1993).

[16] J.P. Perdew, K. Burke, Y. Wang, *Phys. Rev. B* **54**, 16533 (1996).

[17] A.D. Becke II, *J. Chem. Phys.* **98**, 5648 (1993).

[18] S.H. Vosko, L. Wilk, M. Nusair II, *Can. J. Phys.* **58**, 1200 (1980).

[19] J.P. Perdew II, *Phys. Rev. B* **33**, 8822 (1986).

[20] K.B. Wiberg, *Tetrahedron* **24**, 1083 (1968).

[21] F Weinhold, C.R. Landis, *Valency and bonding: a natural bond order donor acceptor perspective*, Cambridge University Press, UK (2005).

[22] M.H. Jamroz, *Vibrational Energy Distribition Analysis (VEDA 4) Program*, Warsaw, Poland, (2004).

[23] T. Sivaranjani, S. Periandy, S. Xavier, *J. Mol. Struct.* **1108**, 398 (2016).

[24] T. Prabhu, S. Periandy, S. Ramalingam, *Spectrochim. Acta A* **83**, 8 (2011).

[25] I.M. Alecu, J. Zheng, Y. Zhao, D.G. Truhlar, *J. Chem. Theory. Comput.* **6**, 2872 (2010).

[26] T. Lu, F. Chen, *J. Comput. Chem.* **33**, 580 (2012).

[27] W. Humphrey, A. Dalke, K. Schulten, *J. Mol. Graph.* **14**, 33 (1996).

[28] S. Altürk, D. Avcı, Ö. Tamer, Y. Atalay, *Comput. Theor. Chem.* **1100**, 34 (2017).

[29] U.H. Patel, S.A. Gandhi, B.D. Patel, R.D. Modh, R.H. Patel, J. Yadav, K.R. Desai, *Indian J. Pure Appl. Phys.* **51**, 819 (2013).

[30] S.L. Dhonnar, B.S. Jagdale, A.B. Sawant, T.B. Pawar, S.S. Chob, *Der Pharma Chemica* **8**, 119 (2016).

[31] R.J. Butcher, M. Akkurt, S. Samshuddin, B. Narayana, H.S. Yathirajan, *Acta Crystallogr. E* **67**, 1346 (2011).

[32] M. Sekar, R. Velmurugan, A. Chandramohan, P. Rameshb, M.N. Ponnuswamy, *Acta Cryst. E* **67**, 3270 (2011).

[33] K. Carthigayan, S. Xavier, S. Periandy, *Spectrochim. Acta A* **142**, 350 (2015).

[34] W. Huang, H. Qian, *Dyes Pigments* **77**, 446 (2008).

[35] Ö. Alver, M.F. Kaya, M. Bilge, C. Parlak, *J. Theor. Chem.* **2013**, 1 (2013).

[36] P.M. Anbarasan, M.K. Subramanian, P. Senthilkumar, C. Mohanasundaram, V. Ilangovan, N. Sundaraganesan, *J. Chem. Pharm. Res.* **3**, 597 (2011).

[37] I.M. Alecu, J. Zheng, Y. Zhao, D.G. Truhlar, *J. Chem. Theory. Comput.* **6**, 2872 (2010).

[38] T. Prabhu, S. Periandy, S. Ramalingam, *Spectrochim. Acta A* **83**, 8 (2011).

[39] A. Eşme, S.G Sağdınç, *Acta Phys. Pol. A* **130**, 1273 (2016).

[40] G. Varsanyi, *Assignment for Vibrational Spectra of Seven Hundred Benzene Derivatives*, Academic Kiaclo, Budapest 1973.

[41] S. Muthu, J.U. Maheswari, *Spectrochim. Acta A* **92**, 154 (2012).

[42] A. Eşme, *Indian J. Pure Appl. Phys.* **55**, 478 (2017).

[43] D. Sajan, J. Binoy, B. Pradeep, K.V. Krishnan, V.B. Kartha, I.H. Joe, V.S. Jayakumar, *Spectrochim Acta A* **60**, 173 (2004).

[44] M. Ristova, L. Pejov, M. Zugic, B. Soptrajanov, *J. Mol. Struct.* **482**, 647 (1999).

[45] M. Karabacak, E. Postalcilar, M. Cinar, *Spectrochim. Acta A* **85**, 261 (2012).

[46] G. Socrates, *Infrared and Raman Characteristic Frequencies*, Wiley, New York 2001..

[47] M. Silverstein, G.C. Basseler, C. Morill, *Spectrometric Identification of Organic Compounds*, Wiley, New York 1981.

[48] Y. Sert, M. Gümüş, V. Kamaci, H. Gökce, İ. Kani, İ. Koca, *J. Theor. Comput. Chem.* **16**, 1750039 (2017).

[49] R. Aquel, P.K. Verma, *Indian J Pure Appl Phys* **20**, 665 (1982).

[50] M. Evecen, H. Tanak, F. Tinmaz, N. Dege, I.O. Ilhan, *J. Mol. Struct.* **1126**, 117 (2016).

[51] A.J. LaPlante, H.D. Stidham, *Spectrochim. Acta A* **74**, 808 (2009).

[52] G. Varsanyi, *Assignments of Vibrational Spectra of FOD Benzene Derivatives*, Wiley, New York 1974.

[53] I. Fleming, *Frontier Orbitals and Organic Chemical Reactions*, Wiley, London 1976.

[54] N.M. O'Boyle, A.L. Tenderholt, K.M. Langner, *J. Comput. Chem.* **29**, 839 (2008).

[55] T.C. Koopmans, *Physica (Amsterdam)* **1**, 104 (1934).

[56] A. Eşme, S.G. Sağdınç, *Spectrochim. Acta A* **188**, 443 (2018).

[57] P. Politzer, J. Murray, *Theor. Chem. Acc.* **108**, 134 (2002).

[58] J.K.M. Sanders, B.K. Hunter, *Modern NMR Spectroscopy. A Guide for Chemists*, Oxford University Press, Oxford 1987.

[59] M. Govindarajan, M. Karabacak, *Spectrochim Acta A* **96**, 421 (2012).

[60] B.L. Shapiro, L.E. Mohrmann, *J. Phys. Chem. Ref. Data* **6**, 919 (1977).

[61] M.E. Castro, M.J.Percino, V.M. Chapela, M. Ceron, G. Soriano-Moro, J. Lopez-Cruz, F.J. Melendez, *Int. J. Mol. Sci.* **14**, 4005 (2013).

[62] S. Xavier, S. Periandy, *Spectrochim Acta A* **149**, 216 (2015).

[63] H. Vural, *J. Mol. Struct.* **1111**, 55 (2016).

[64] D.A. Kleinman, *Physics Reviews* **126**, 1977 (1962).

[65] P. Karamanis, C. Pouchan, G. Maroulis, *Phys. Rev. A* **77**, 013201 (2008).

[66] S.G. Sagdinc, A. Eşme, *Spectrochim. Acta A* **75**, 1370 (2010).

[67] Ü. Ceylan, G.Ö. Tarı, H. Gökçe, E. Ağar, *J. Mol. Struct.* **1110**, 1 (2016).

[68] C. Cassidy, J.M. Halbout, W. Donaldson, C.L.Tang, *Opt. Commun.* **29**, 243 (1979).

[69] E.R. Johnson, S. Keinan, P. Mori-Sanchez, J. Contreras-Garcia, A.J. Cohen, W. Yang, *J. Am. Chem. Soc.* **132**, 6498 (2010).